2020 3rd IEEE International Conference on Soft Robotics (RoboSoft)
Yale University, USA

Electromechanical Characterization of 3D Printable Conductive Elastomer for Soft Robotics

Suhan Kim, Sukjun Kim, Houriyeh Majditehran, Dinesh K. Patel, Carmel Majidi and Sarah Bergbreiter

***Abstract*— Soft, stretchable sensors, such as artificial skins or tactile sensors, are attractive for numerous soft robotic applications due to the low material compliance. Conductive polymers are a necessary component of many soft sensors, and this work presents the electromechanical characterization of 3D-printable conductive polymer composites. Dog-bone shaped samples were 3D printed using a digital light processing (DLP)-based 3D printer for characterization. The 3D printable resin consists of monomer, crosslinker, conductive nano-filler, and a photo-initiator. The characterization was performed in two tracks. First, the effect of two different crosslinkers was investigated with different compositions and second, the effect of concentration of conductive nano-fillers was explored. Crosslinkers were chosen by referring to previous studies, and carbon nanotubes (CNTs) were utilized as conductive nano-fillers. The samples were 3D printed and characterized using an electromechanical test setup. To demonstrate utility for 3D printed soft robotics, a capacitance-based joystick sensor composed of both conductive and non-conductive resins was 3D printed.**

I. INTRODUCTION

Soft robotic systems enable compliant and dexterous mechanisms, which used to overcome numerous challenges seen in conventional rigid robots [1]. In most cases, fabrication of soft robotics still require numerous manual steps because of the difficulty in handling the elastomeric materials. One way to overcome this challenge is to use additive manufacturing techniques, commonly referred as 3D printing, for the fabrication of soft robots [2], [3], [4]. 3D printing can integrate and automate multiple separate fabrication steps, starting from design to assembly [5], [6]. Furthermore, 3D printing can enable the fabrication of more complex geometries, which would be challenging to achieve using conventional fabrication methods like molding [7].

3D printing methods for polymers can be categorized into two types based on how the polymer is cured: thermal curing methods and photocuring (in most cases UV curing) methods. Fused deposition modeling (FDM) or selective laser sintering (SLS) 3D printers are well-known techniques which take advantage of thermoplastic polymers [5], [6], [8]. Stereolithography (SLA) [9] and digital light processing (DLP)-based 3D printing [10], [11], [12] exploit the photo-crosslinking formulations of elastomers. Pros and cons of each depend on the objectives of printing, but when constructing complex structures, SLA or DLP type 3D printing has great advantages, since the size of the targeted curing volume is much smaller. This ultimately leads to higher resolution printed structures [9], [13].

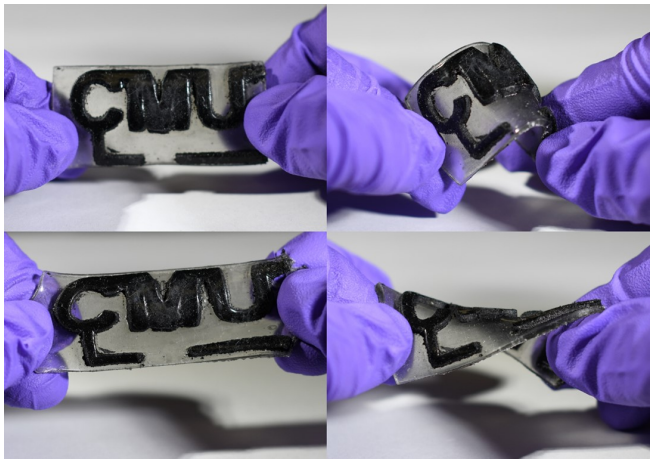

Fig. 1. Demonstration of multi-material 3D printing technique capable of printing conductive elastomers. 3D printed CMU logo (top left) showing flexibility by bending (top right), stretching (bottom left), and twisting (bottom right) the sample.

3D printers that use photocurable resins also allow the resin to be modified to add functionality [14], [15], [16]. Various types of functionalities have been added to photocurable resins including electrical conductivity [17], [18], [19], magnetization [20], [21], or shape memory effects [22], [23], [24]. Many of these approaches have resulted in more rigid materials however. In order to achieve 3D printed functional materials that also have low modulus for soft robotics, it is important to study a variety of approaches to fabricate these materials. For example, to make conductive soft materials, a common approach is to add conductive fillers, such as silver particles [17], [18], graphene [25], [26], carbon black [19], [27], or carbon nano-tubes (CNTs) [28], [29] to the polymers before polymerization.

This study investigates the mechanical and electrical properties of 3D printed conductive elastomers for use in soft sensors for soft robotics. Soft sensors often use both conductive soft materials as well as dielectric soft materials requiring printing with multiple materials. In this paper, a DLP 3D printer was utilized, and multi-walled carbon nanotubes (MWCNTs) were chosen as a conductive nanofiller. Previous studies investigated the formulation of 3D printable conductive polymer using DLP technique [10],

This research was initiated as the course project of Soft Robotics (24-673) under the guidance of Prof. Carmel Majidi, and primarily supported by the Department of Mechanical Engineering in Carnegie Mellon University (CMU).

Upon the progress, the research effort was also supported by the National Science Foundation (NSF) award number BCS-1921251

The authors are with the Department of Mechanical Engineering, Carnegie Mellon University, Pittsburgh, PA, USA. Corresponding author: Prof. Sarah Bergbreiter (sbergbre@andrew.cmu.edu)

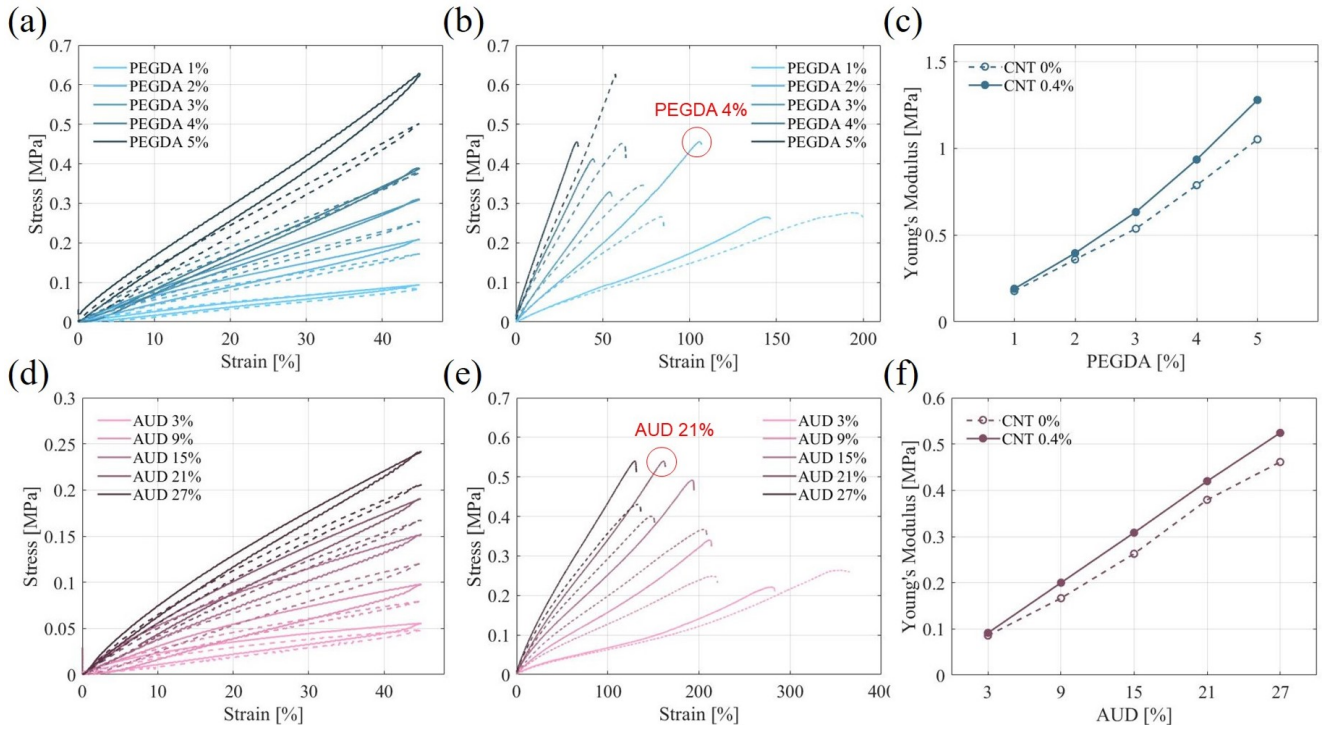

Fig. 2. The results of mechanical characterization: (a) cyclic load test result of PEGDA/EAA samples (b) breaking test result of PEGDA/EAA samples (c) Young's Modulus to PEGDA concentration (d) cyclic load test result of AUD/EAA samples (e) breaking test result of AUD/EAA samples (f) Young's Modulus to AUD concentration. The results were plotted in the same manner that the darker colors represent the result of higher composition of crosslinkers (PEGDA and AUD). Also, the solid and dashed line show the result of 0.4 wt% CNTs and 0 wt% CNTs respectively.

and furthermore demonstrated multi-material printing using similar principle [30]. The work in this paper introduces a novel combination of 3D printable polymer composites to obtain high stretchability – a common challenge in previous studies. We expect mechanical and electrical properties to change with different crosslinkers as well as different compositions of polymer and filler particle. Preparation of the printing resins is described, and electrical and mechanical characterization results were compared for different resin compositions. Finally, a joystick-like sensor is printed and tested.

II. MATERIALS AND METHODS

A. Material

The resin for photocurable, or UV-curable, polymer consists of monomers, crosslinkers, and photo-initiators. Epoxy aliphatic acrylate (EAA, Ebecryl 113, Allnex) was used as monomer, and two different crosslinkers, aliphatic urethane diacrylate (AUD, Ebecryl 8411, Allnex) and poly(-ethylene glycol) diacrylate (PEGDA, average M_n = 250 g/mol, Sigma Aldrich), were chosen by referring to previous studies [10], [11].

Multi-walled carbon nano-tubes (MWCNTs, Cheaptubes) with an outer diameter of less than 8 *nm* and an inner diameter of 2 to 5 *nm* were used as a filler particle to achieve electrical conductivity. The length of MWCNTs ranged from 10 to 30 μm. Different compositions of photoinitiators were applied, bis (2,4,6-trimethyl benzoyl)-phosphine oxide (Irgacure 819, Rahn) with 1-Hydroxy-cyclohexyl-phenyl-ketone (Irgacure 184, Rahn) for the resin containing CNTs, and diphenyl (2,4,6-trimethyl benzoyl)-phosphine oxide (TPO, Rahn) for the resin without CNTs.

B. Sample preparation

Both non-conductive and conductive resins were prepared. For the conductive resin, CNTs were added and dispersed to half of the EAA monomer using an ultrasonic liquid processor (VCX 500, Sonics). The dispersion was performed for 30 minutes with an intensity of 250 W under pulse operation (2 sec on and 2 sec off) to prevent the solution from overheating. Crosslinkers (PEGDA and AUD) and photoinitiators (2 wt% of Irgacure 819 with 4 wt% of Irgacure 184) were added to the other half of the EAA monomer and mixed on a hot plate with a magnetic stirrer (SP88857100, Thermo-scientific) until the photoinitiators were fully dissolved. The temperature and speed were set to 80 °C and 600 RPM respectively. Then, both solutions were mixed together using magnetic stirring at 80 °C and 600 RPM for another 20 minutes. The non-conductive resin was prepared similarly, but without the CNTs and used 2 wt% of TPO as a photoinitiator.

The range of PEGDA concentration was determined after a brief evaluation of the ductility of polymerized samples. It was observed that PEGDA/EAA polymers with higher than 5% of PEGDA concentration showed very low stretchability compared to typical elastomers. Therefore, the concentration range of PEGDA was set to be from 1 wt% to 5 wt%, with an increment of 1 wt%. The range of AUD concentration

was determined from the conductivity. AUD/EAA polymer samples with 30 wt% of AUD concentration had very low conductivity, showing gigaOhms of resistance. Thus, the concentration of AUD was set to range from 3 wt% to 27 wt%, with a 6 wt% increment. The concentration of CNTs was fixed to 0.4 wt% which were optimized for 3D printing and for the conductivity.

A DLP based 3D printer Asiga pico 2 HD (Asiga) was used for sample fabrication. The main printing parameters were the exposure time of UV light and the layer thickness. The exposure time and the layer thickness were set as 5 s and 100 μm for the samples without CNTs, and 20 s and 25 μm for the ones containing CNTs. The geometry of the printed sample followed the ASTM standard dogbone shape [31], but scaled down by 1/6 to fit within the building platform of 3D printer. When printing the conductive samples, 100 μm of the non-conductive initial layer was printed beforehand to provide better adhesion between the sample and the building platform. For the initial non-conductive layer, the resin with the same crosslinker composition was used. Finally, printed samples were post-processed by sonication (CPX 3800, Branson) in isopropyl alcohol (IPA) for 2 minutes, and post-curing in UV chamber (DR-301C, Asiga) for 3 minutes.

C. Characterization

Copper tape was used to make electrical connection to the sample, and silver epoxy was used between the sample and the copper tape to minimize contact resistance. The ends of the sample were covered with masking tape, which also provided consistent friction between the sample and the testing system. The electrical conductivity of the samples was primarily measured using a digital multimeter (34461A, Keysight).

The electromechanical characterization was performed using a universal testing system (5969, Instron, 10 N load cell) integrated with a voltage divider. The reference resistor for the voltage divider was selected by matching up the resistance of the sample to maximize the sensitivity. Both the universal testing system and voltage divider circuit was connected to the data acquisition processor (NI DAQ, National Instrument) which enabled synchronized data acquisition.

Two different tests were performed for each sample. For the cyclic load test, aa maximum strain of 45 % was applied. One cycle in this test consisted of ramp loading and unloading at 60 mm/min, and the load was applied for 10 cycles. The second test was the tensile breaking test with a constant velocity of 10 mm/min until mechanical failure. The resistance of the samples was measured from the voltage divider circuit during both tests.

III. RESULTS

A. Mechanical properties

Figure 2 (a)-(c) show the mechanical characterization results of PEGDA/EAA polymers, and (d)-(f) are the results from AUD/EAA polymers. Figure 2 (a) shows the cyclic load test results along with the different composition of PEGDA. It is observed that a higher PEGDA concentration increases

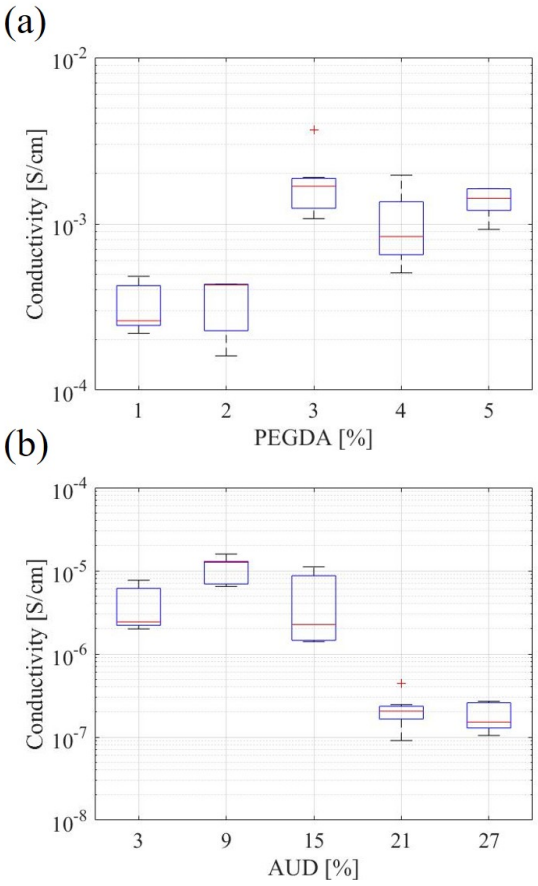

Fig. 3. Electrical conductivity of 0.4 wt% CNTs samples with varying crosslinker concentrations: (a) conductivity to PEGDA concentration, (b) conductivity to AUD concentration

the mechanical stiffness; the maximum stress for the PEGDA sample with 5 wt% was over 6x larger than the maximum stress for the 1 wt % PEGDA sample. Also, in each PEGDA concentration, samples with 0.4 wt% CNTs showed higher stiffness than the samples not containing CNTs. Same trend was also observed during the tensile breaking test (Figure 2 (b)). Furthermore, increasing the PEGDA ratio decreased the elongation at the break. In each PEGDA composition, samples without CNTs showed longer elongation range than the ones with 0.4 wt% CNTs. While most of the samples followed the trend, the sample with 4 wt% PEGDA was an outlier, showing the higher elongation range when CNTs are added.

AUD/EAA samples showed a similar trend to that in PEGDA/EAA samples; adding AUD increased the mechanical stiffness, and the samples with 0.4 wt% CNTs showed higher stiffness than those with 0 wt% CNTs (Figure 2 (d)). The higher concentration of AUD and the presence of CNTs also reduced the maximum elongation, but samples of 21 wt% AUD were an exception. At 21 wt% AUD 0.4 wt% CNTs samples showed higher maximum elongation than 0 wt% CNTs samples. Figure 2 (c) and (f) show Young's modulus along the concentration of PEGDA and AUD for both 0 wt% and 0.4 wt% CNTs samples. The graph

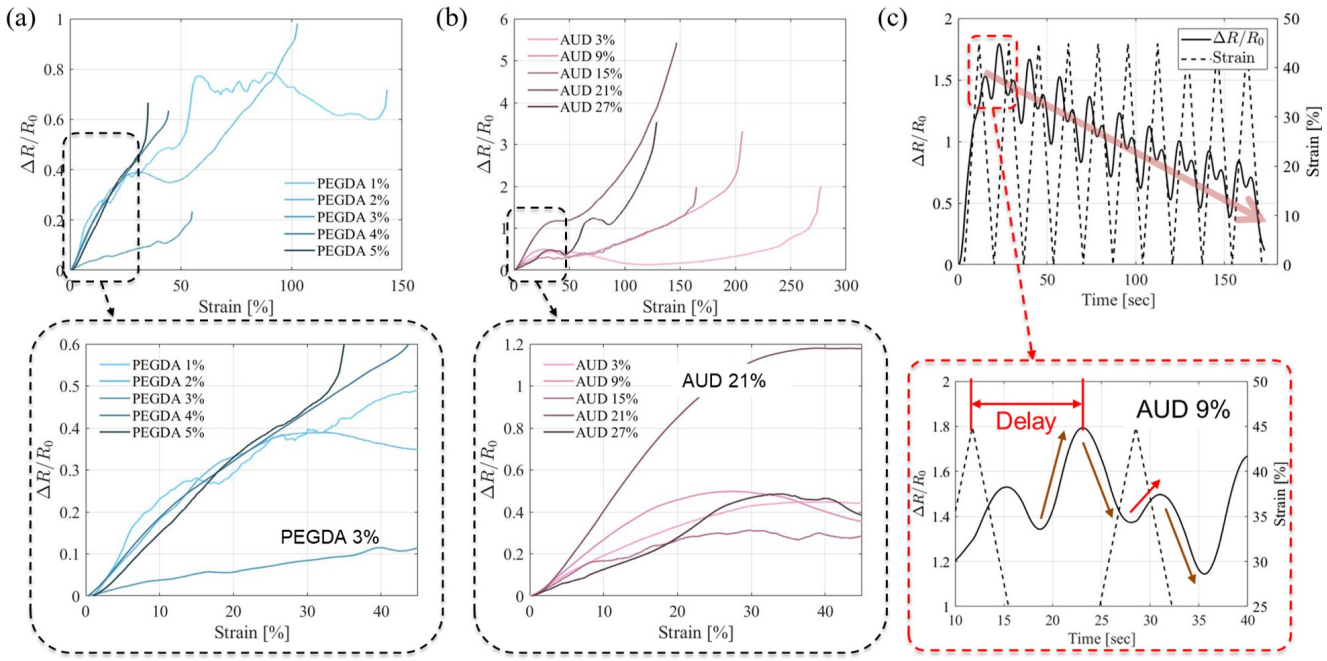

Fig. 4. The results of electromechanical characterization: (a) resistance to strain response in breaking test of (a) PEGDA/EAA samples and (b) AUD/EAA samples, and (c) cyclic test with the sample with 9 wt% of AUD

clearly demonstrates the positive effect of the crosslinker concentration to Young's modulus. The plot also presents the effect of adding CNTs by the gap between the solid line and dashed line. Overall, PEGDA/EAA shows the higher mechanical stiffness while AUD/EAA shows the higher elongation limits.

The effect of nano-fillers in stiffness of the material has been studied with various elastomer composites [32], [33]. To qualitatively describe the possible reason, solid fillers perturb the stresses and strains, which causes the elastic energy of the material to increase. This ultimately induces the higher mechanical stiffness.

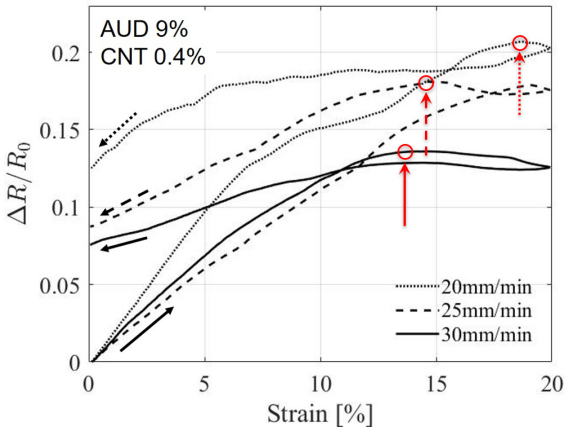

Fig. 5. Resistance response of 9 wt% AUD conductive sample along with 20% ramp strain input in three different loading speed (20, 25, and 30 mm/min). Red circles and arrows represent the peak of the resistance change

Previous research demonstrated that higher concentrations of AUD crosslinker increases the mechanical stiffness [11], and the results in this paper show strong agreement with that finding. A higher cross-linking density causes a tighter knit polymer network which results in the higher stiffness. A similar result was reported for polydimethylsiloxane (PDMS) [34] which provides validations to those qualitative claims. However, the opposite phenomenon was also observed that higher crosslinker composition decreased Young's modulus [35], [36]. In those cases, an excessive amount of crosslinker lead to voids or a dilution of the polymer network, while the crosslinker saturates locally inside the material.

B. Conductivity

Figure 3 shows the conductivity of the polymers with the two crosslinkers. 7 to 10 samples of each composition with 0.4 wt% CNTs were printed and measured. Data is displayed using a box plot. PEGDA/EAA samples showed around $10^{-3}S/cm$ of conductivity, with a slight increment after 3 wt% of PEGDA ratio. However, despite the similar composition, samples with 3 wt% AUD had much lower conductivity (around $10^{-5}S/cm$) compared to the 3 wt% PEGDA polymer composite. Furthermore, it was observed that when more than 21 wt% of AUD was added, conductivity dropped drastically to around $10^{-7}S/cm$, which demonstrates the negative effect of AUD on the conductivity.

C. Electromechanical response

Resistance to strain response upon the mechanical failure was presented to show the electromechanical behavior of the printed conductive elastomer. The resistance of PEGDA/EAA samples linearly increased up to 30 % strain,

with most of the samples showing a similar proportion. However, the sample with 3 wt% PEGDA had an irregular resistance to strain ratio compared to the other samples, about 4 times lower than the others.

In the resulting plot of AUD/EAA (Figure 4 (b)) the resistance increased linearly to the strain in 20 % strain range. In this case, the samples with 21 wt% AUD showed higher slope while the other samples stayed within a similar range. After the linear region, a similar trend was observed for most of the AUD/EAA samples that the resistance primarily saturated, or even descended in a slow rate, then increased again until the failure. The resistance showed a stiff increase at the end, which indicates the start of mechanical failures.

Nonlinear behavior of electromechanical response in Figure 4 (b) was also observed in previous studies which used carbon black or MWCNTs as the nano-fillers [37], [38]. The resistance response while stretching is due to two different effects in the filler network. As the sample starts to stretch, the percolation network between filler particles starts to break, resulting in increased resistance. However, once the stretch reaches a certain level, the filler aggregates and aligns in the stretching direction, reformulating the filler networks. As a result, the conductivity recovers in higher strain region which results in a decrease in resistance.

The result of electromechanical characterization from the cyclic test is shown in Figure 4 (c). The result using the sample with AUD 9 wt% and CNTs 0.4 wt% were presented due to its higher elongation at break. The cyclic load was applied with a speed of 60 mm/min for 10 cycles.

Three interesting features were observed in the result. First, the resistance response was not monotonic showing some regions where the resistance increased while strain decreased (or in the opposite direction). The non-monotonic response of the resistance can be attributed to the breakage and reforming of the filler network as described above. Second, a delay in electrical response was observed that the highest strain was followed by the peak of the resistance after a certain amount of time gap. Finally, after the first stretch, the resistance recovered slowly to its initial value. To investigate the effect of the dynamic loading condition deeper, the cyclic load tests with various loading and unloading speeds were conducted (Figure 5). The speeds were 20, 25, and 30 mm/min respectively. When the speed was 20 mm/min, the delay of the electrical response (the gap between strain peak and resistance peak) and non-monotonic response were barely observed. This result demonstrates the time-dependent behaviors in the electromechanical response of CNTs added to elastomers.

IV. MULTI-MATERIAL SENSOR DESIGN

A multi-material based joystick was 3D printed. The entire structure was 3D printed using the same 3D printer. It consists of three different materials: the conductive and non conductive elastomers studied above, along with a rigid material. The structure has four flexible capacitors at the bottom (Figure 6 (a)), which also function as a mechanical suspension for the joystick movement.

5 wt% PEGDA with 0.4 wt% CNT composition was chosen considering its conductivity and mechanical property, and a non-conductive sample with 4 wt% PEGDA was opted for dielectric layer fabrication. The rigid ink was formulated by integrating EAA, AUD and Tripropyleneglycoldiacrylate (TPGDA, Sigma Aldrich) in the weight ratio of 3:3:4. 0.6 wt% TPO was added as photo-initiator and the resin was colored using 0.15 wt% of Rhodamine dye. Since the resin of rigid material contained EAA as its composite, it also enhanced the adhesion between the rigid part and flexible part during the printing process.

Capacitors were designed as two parallel electrodes with 200 μm gap in between. Assuming that the dielectric constant of 4 wt% PEGDA sample lies in the range of typical dielectric constants of polymers (2.5 - 3.9), each capacitor module would have the nominal capacitance of 2.17 - 3.39 pF. The actual prototype showed 3.216 pF as the average of four capacitors, demonstrating good agreement with the prediction. A commercial capacitance evaluation board (AD7746, Analog Devices) was utilized to measure

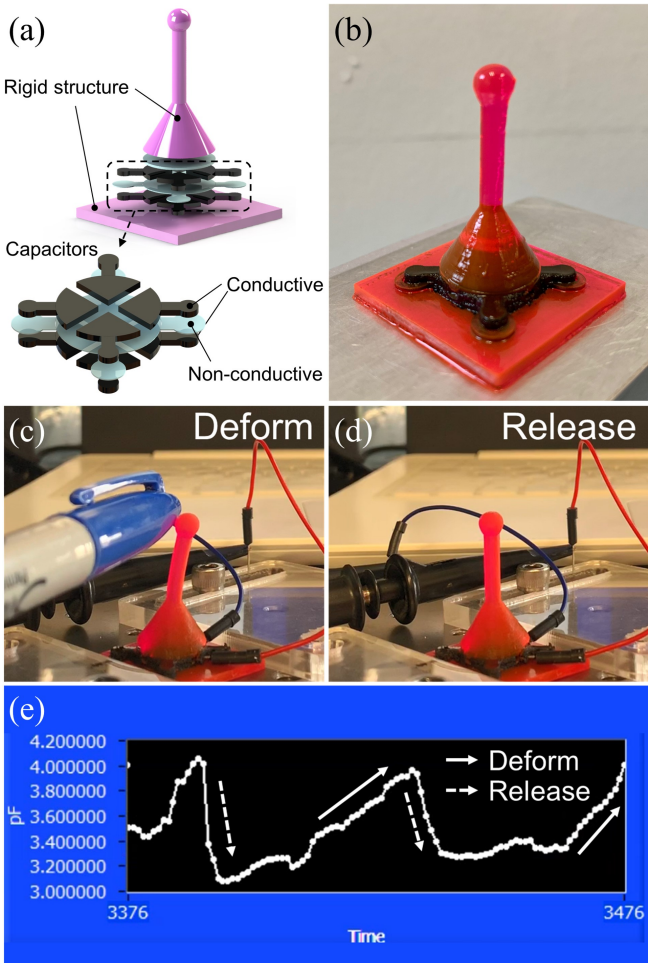

Fig. 6. Design, fabrication, and testing of capacitive based joystick. (a) Schematic of the joystick structure with capacitive transduction design, (b) fabricated prototype with fully 3D-printing, (c-d) testing scene of joystick with its deformed and released state, and (e) capacitance response of the capacitance module.

capacitances. Figure 6 (c)-(e) shows both the deformed shape of the joystick and corresponding capactiance change. The capacitance remained around 3.2-3.4 pF when the joystick is in rest position, but when the joystick was deflected, the capacitance increased to the 3.9 - 4.1 pF range.

V. CONCLUSIONS

In this research, 3D printable conductive elastomers for soft robotics were characterized by their electromechanical properties. Samples were prepared using two different crosslinkers (PEGDA and AUD), with varying composition. Conductivity was achieved by adding CNTs as nano-fillers, and the effect of the presence of CNTs were also investigated. Scaled dogbone shape samples were fabricated using DLP 3D printer, and tensile load tests with resistance measurements were performed to characterize the electromechanical behavior.

The result showed that both the crosslinkers and CNTs enhance the mechanical stiffness while decreasing the maximum elongations. During the investigation of mechanical properties, it was also found out that addition of PEGDA noticeably affects the ductility, which could be observed by comparing the elongation range of PEGDA/EAA polymer with AUD/EAA polymer. Increasing the composition of AUD affected the conductivity. A significant drop of electrical conductivity was observed after adding more than 21 wt% of AUD.

Overall, the results showed a certain level of agreement with previous studies which exploited DLP 3D printing of elastomeric materials as well as studies that investigated CNTs added polymers. Taking advantage of the result, a capacitive transduction joystick sensor was 3D printed using a multi-material process and was demonstrated. This characterization and early demonstration shows the promise for integrating these soft, 3D printed materials into more complex soft sensors and soft robotics in the future.

ACKNOWLEDGMENT

This work was supported by the National Science Foundation award number BCS-1921251. Resources for this work were also provided by Prof. Carmel Majidi (Soft Machines Lab, SML) and Prof. Sarah Bergbreiter (Micro Robotics Lab, MRL). We also thank Jiahe Liao for assistance with this research.

REFERENCES

[1] C. Majidi, "Soft-matter engineering for soft robotics," *Advanced Materials Technologies*, vol. 4, no. 2, p. 1800477, 2019.

[2] J. W. Stansbury and M. J. Idacavage, "3d printing with polymers: Challenges among expanding options and opportunities," *Dental Materials*, vol. 32, no. 1, pp. 54–64, 2016.

[3] J. Z. Gul, M. Sajid, M. M. Rehman, G. U. Siddiqui, I. Shah, K.-H. Kim, J.-W. Lee, and K. H. Choi, "3d printing for soft robotics–a review," *Science and technology of advanced materials*, vol. 19, no. 1, pp. 243–262, 2018.

[4] T. Wallin, J. Pikul, and R. Shepherd, "3d printing of soft robotic systems," *Nature Reviews Materials*, vol. 3, no. 6, p. 84, 2018.

[5] H. Lipson, F. C. Moon, J. Hai, and C. Paventi, "3-d printing the history of mechanisms," *Journal of Mechanical Design*, vol. 127, no. 5, pp. 1029–1033, 2005.

[6] P. F. Jacobs, *Rapid prototyping & manufacturing: fundamentals of stereolithography*. Society of Manufacturing Engineers, 1992.

[7] D. H. Freedman, "Layer by layer," *Technology Review*, vol. 115, no. 1, pp. 50–53, 2012.

[8] J. V. Crivello and E. Reichmanis, "Photopolymer materials and processes for advanced technologies," *Chemistry of Materials*, vol. 26, no. 1, pp. 533–548, 2013.

[9] S. Kirihara, "Additive manufacturing of ceramic components using laser scanning stereolithography," *Welding in the World*, vol. 60, no. 4, pp. 697–702, 2016.

[10] G. Gonzalez, A. Chiappone, I. Roppolo, E. Fantino, V. Bertana, F. Perrucci, L. Scaltrito, F. Pirri, and M. Sangermano, "Development of 3d printable formulations containing cnt with enhanced electrical properties," *Polymer*, vol. 109, pp. 246–253, 2017.

[11] D. K. Patel, A. H. Sakhaei, M. Layani, B. Zhang, Q. Ge, and S. Magdassi, "Highly stretchable and uv curable elastomers for digital light processing based 3d printing," *Advanced Materials*, vol. 29, no. 15, p. 1606000, 2017.

[12] I. Cooperstein, M. Layani, and S. Magdassi, "3d printing of porous structures by uv-curable o/w emulsion for fabrication of conductive objects," *Journal of Materials Chemistry C*, vol. 3, no. 9, pp. 2040–2044, 2015.

[13] R. D. Farahani, M. Dubé, and D. Therriault, "Three-dimensional printing of multifunctional nanocomposites: manufacturing techniques and applications," *Advanced Materials*, vol. 28, no. 28, pp. 5794–5821, 2016.

[14] M. Lukić, J. Clarke, C. Tuck, W. Whittow, and G. Wells, "Printability of elastomer latex for additive manufacturing or 3d printing," *Journal of Applied Polymer Science*, vol. 133, no. 4, 2016.

[15] M. Schmid and K. Wegener, "Additive manufacturing: polymers applicable for laser sintering (ls)," *Procedia Engineering*, vol. 149, pp. 457–464, 2016.

[16] H. Amel, J. Rongong, H. Moztarzadeh, and N. Hopkinson, "Effect of section thickness on fatigue performance of laser sintered nylon 12," *Polymer Testing*, vol. 53, pp. 204–210, 2016.

[17] H. Jiang, K.-s. Moon, Y. Li, and C. Wong, "Surface functionalized silver nanoparticles for ultrahigh conductive polymer composites," *Chemistry of Materials*, vol. 18, no. 13, pp. 2969–2973, 2006.

[18] S. H. Jeong, S. Y. Yeo, and S. C. Yi, "The effect of filler particle size on the antibacterial properties of compounded polymer/silver fibers," *Journal of Materials Science*, vol. 40, no. 20, pp. 5407–5411, 2005.

[19] M. C. Lonergan, E. J. Severin, B. J. Doleman, S. A. Beaber, R. H. Grubbs, and N. S. Lewis, "Array-based vapor sensing using chemically sensitive, carbon black- polymer resistors," *Chemistry of Materials*, vol. 8, no. 9, pp. 2298–2312, 1996.

[20] L. K. Lagorce, O. Brand, and M. G. Allen, "Magnetic microactuators based on polymer magnets," *Journal of Microelectromechanical Systems*, vol. 8, no. 1, pp. 2–9, 1999.

[21] C. S. Owen, J. C. Silvia, L. D'angelo, and P. A. Liberti, "Magnetic-polymer particles," Jan. 3 1989, uS Patent 4,795,698.

[22] P. T. Mather, X. Luo, and I. A. Rousseau, "Shape memory polymer research," *Annual Review of Materials Research*, vol. 39, pp. 445–471, 2009.

[23] W. Huang, B. Yang, L. An, C. Li, and Y. Chan, "Water-driven programmable polyurethane shape memory polymer: demonstration and mechanism," *Applied Physics Letters*, vol. 86, no. 11, p. 114105, 2005.

[24] T. Xie, "Tunable polymer multi-shape memory effect," *Nature*, vol. 464, no. 7286, p. 267, 2010.

[25] H. Kim, A. A. Abdala, and C. W. Macosko, "Graphene/polymer nanocomposites," *Macromolecules*, vol. 43, no. 16, pp. 6515–6530, 2010.

[26] R. Verdejo, M. M. Bernal, L. J. Romasanta, and M. A. Lopez-Manchado, "Graphene filled polymer nanocomposites," *Journal of Materials Chemistry*, vol. 21, no. 10, pp. 3301–3310, 2011.

[27] I. Balberg, "A comprehensive picture of the electrical phenomena in carbon black–polymer composites," *Carbon*, vol. 40, no. 2, pp. 139–143, 2002.

[28] R. Andrews and M. Weisenberger, "Carbon nanotube polymer composites," *Current Opinion in Solid State and Materials Science*, vol. 8, no. 1, pp. 31–37, 2004.

[29] A. Sharma, S. Kumar, B. Tripathi, M. Singh, and Y. Vijay, "Aligned cnt/polymer nanocomposite membranes for hydrogen separation," *international journal of hydrogen energy*, vol. 34, no. 9, pp. 3977–3982, 2009.

[30] Q. Mu, L. Wang, C. K. Dunn, X. Kuang, F. Duan, Z. Zhang, H. J. Qi, and T. Wang, "Digital light processing 3d printing of conductive complex structures," *Additive Manufacturing*, vol. 18, pp. 74–83, 2017.
[31] A. International, "Astm d638-14 standard test method for tensile properties of plastics," 2014.
[32] H. Lorenz, J. Fritzsche, A. Das, K. Stöckelhuber, R. Jurk, G. Heinrich, and M. Klüppel, "Advanced elastomer nano-composites based on cnt-hybrid filler systems," *Composites Science and Technology*, vol. 69, no. 13, pp. 2135–2143, 2009.
[33] J. Fritzsche, H. Lorenz, and M. Klueppel, "Cnt based elastomer-hybrid-nanocomposites with promising mechanical and electrical properties," *Macromolecular Materials and Engineering*, vol. 294, no. 9, pp. 551–560, 2009.
[34] Z. Wang, A. A. Volinsky, and N. D. Gallant, "Crosslinking effect on polydimethylsiloxane elastic modulus measured by custom-built compression instrument," *Journal of Applied Polymer Science*, vol. 131, no. 22, 2014.
[35] E. A. Wilder, S. Guo, S. Lin-Gibson, M. J. Fasolka, and C. M. Stafford, "Measuring the modulus of soft polymer networks via a buckling-based metrology," *Macromolecules*, vol. 39, no. 12, pp. 4138–4143, 2006.
[36] J.-H. Seo, K. Sakai, and N. Yui, "Adsorption state of fibronectin on poly (dimethylsiloxane) surfaces with varied stiffness can dominate adhesion density of fibroblasts," *Acta biomaterialia*, vol. 9, no. 3, pp. 5493–5501, 2013.
[37] K. Yamaguchi, J. Busfield, and A. Thomas, "Electrical and mechanical behavior of filled elastomers. i. the effect of strain," *Journal of Polymer Science Part B: Polymer Physics*, vol. 41, no. 17, pp. 2079–2089, 2003.
[38] R. Zhang, H. Deng, R. Valenca, J. Jin, Q. Fu, E. Bilotti, and T. Peijs, "Strain sensing behaviour of elastomeric composite films containing carbon nanotubes under cyclic loading," *Composites Science and Technology*, vol. 74, pp. 1–5, 2013.